This is an open access article published under an ACS AuthorChoice License, which permits copying and redistribution of the article or any adaptations for non-commercial purposes.

ACS Sustainable Chemistry & Engineering

Research Article

Cite This: ACS Sustainable Chem. Eng. 2019, 7, 9525−9536

pubs.acs.org/journal/ascecg

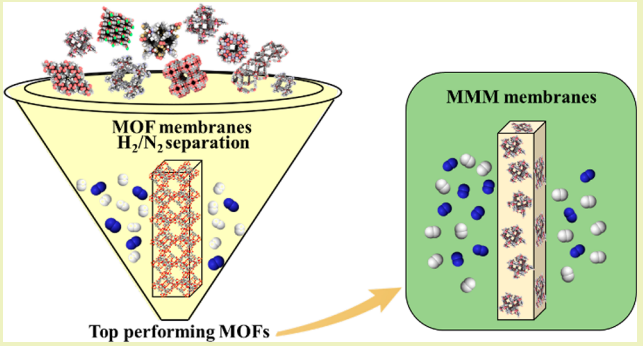
Large-Scale Computational Screening of Metal Organic Framework (MOF) Membranes and MOF-Based Polymer Membranes for H_2/N_2 Separations

Ayda Nemati Vesali Azar, Sadiye Velioglu, and Seda Keskin*

Department of Chemical and Biological Engineering, Koc University, Rumelifeneri Yolu, Sariyer, 34450 Istanbul, Turkey

Supporting Information

ABSTRACT: Several thousands of metal organic frameworks (MOFs) have been reported to date, but the information on H_2/N_2 separation performances of MOF membranes is currently very limited in the literature. We report the first large-scale computational screening study that combines state-of-the-art molecular simulations, grand canonical Monte Carlo (GCMC) and molecular dynamics (MD), to predict H_2 permeability and H_2/N_2 selectivity of 3765 different types of MOF membranes. Results showed that MOF membranes offer very high H_2 permeabilities, 2.5×10^3 to 1.7×10^6 Barrer, and moderate H_2/N_2 membrane selectivities up to 7. The top 20 MOF membranes that exceed the polymeric membranes' upper bound for H_2/N_2 separation were identified based on the results of initial screening performed at infinite dilution condition. Molecular simulations were then carried out considering binary H_2/N_2 and quaternary $H_2/N_2/CO_2/CO$ mixtures to evaluate the separation performance of MOF membranes under industrial operating conditions. Lower H_2 permeabilities and higher N_2 permeabilities were obtained at binary mixture conditions compared to the ones obtained at infinite dilution due to the absence of multicomponent mixture effects in the latter. Structure−performance relations of MOFs were also explored to provide molecular-level insights into the development of new MOF membranes that can offer both high H_2 permeability and high H_2/N_2 selectivity. Results showed that the most promising MOF membranes generally have large pore sizes (>6 Å) as well as high surface areas (>3500 m^2/g) and high pore volumes (>1 cm^3/g). We finally examined H_2/N_2 separation potentials of the mixed matrix membranes (MMMs) in which the best MOF materials identified from our high-throughput screening were used as fillers in various polymers. Results showed that incorporation of MOFs into polymers almost doubles H_2 permeabilities and slightly enhances H_2/N_2 selectivities of polymer membranes, which can advance the current membrane technology for efficient H_2 purification.



KEYWORDS: *Metal organic framework, H_2 purification, H_2/N_2 separation, Molecular simulations, Mixed matrix membrane*

INTRODUCTION

The increasing demand for hydrogen (H_2) production has attracted tremendous interest because H_2 is an efficient energy carrier with zero pollution emission.[1] H_2 should be separated from various gas mixtures, and separation of H_2 from N_2 is specifically important in industrial applications, for example, in carbon black manufacturing where the dry postcombustion gas stream consists of H_2, N_2, CO, and CO_2.[2] The requirement of high purity H_2 has directed the research to membrane-based separation because this process has the advantages of ease of operation and low energy consumption compared to the traditional separation methods such as cryogenic distillation and pressure swing adsorption. Polymeric membranes and dense metallic membranes have been commonly used for H_2 purification.[3,4] Recently, a new class of porous materials, metal organic frameworks (MOFs), have been considered as promising membrane candidates for H_2 purification because of their outstanding gas separation performances, which can overcome the limitations of conventional membrane materials.[5]

MOFs consist of metal complexes connected by organic linkers to form highly porous crystals. They have controllable pore sizes and uniform pore distributions, which can be rationally designed during their synthesis by altering the combination of metals and organic linkers.[5] Although thousands of diverse structures have been synthesized to date, only a small number of MOFs has been tested as membranes for gas separations.[6] Most of the fabricated MOF membranes exhibit high gas permeability, which leads to a reduction both in the required surface area and the capital cost of the membrane-based separation process. Although MOF membranes offer great promise for high H_2 permeability, their

Received: February 20, 2019
Revised: April 4, 2019
Published: April 22, 2019

Downloaded via 85.98.159.57 on March 31, 2020 at 08:26:04 (UTC).
See https://pubs.acs.org/sharingguidelines for options on how to legitimately share published articles.

© 2019 American Chemical Society

DOI: 10.1021/acssuschemeng.9b01020
ACS Sustainable Chem. Eng. 2019, 7, 9525−9536

H_2/N_2 selectivities have been reported to be lower than the desired values. Several well-known MOF membranes such as MOF-5, MIL-53, Ni-MOF-74, and Cuhfb were reported to have ideal H_2/N_2 selectivities in the range of 2.5−4.[7,8] Cu-BTC is one of the most widely studied MOF membranes in the literature, and selectivities of Cu-BTC membranes for separation of H_2/N_2 mixtures varied between 3.7 and 8.9, whereas their ideal selectivities were reported to be 3.7−12.8.[9−12] H_2 and N_2 permeabilities through Cu-BTC membranes were reported to vary within 2 orders of magnitude, 1.6×10^3 to 2.1×10^5 and 1.5×10^2 to 5.7×10^4 Barrer, respectively, both in the single-component and binary gas mixture permeability measurements. These variations may be explained by the usage of different types of membrane preparation procedures to achieve continuous, intergrown, thin MOF membranes having various qualities and hence separation performances.[13]

Zeolitic imidazolate frameworks (ZIFs), a subclass of MOFs, have been also widely studied as membranes. ZIF-8, ZIF-22, ZIF-78, and ZIF-90 membranes were reported to exhibit the highest ideal selectivities (6−16) and mixture selectivities (5−12) among the fabricated MOF membranes for H_2/N_2 separation.[14−21] H_2 and N_2 permeabilities of ZIF membranes were also reported to be high, 3.6×10^3 to 2.4×10^4 and 5.4×10^2 to 3.5×10^3 Barrer, respectively. At that point, it is important to note that H_2/N_2 selectivities reported for MOF membranes are lower than the ideal selectivities of polymeric membranes, which vary between 2 and 300.[3] However, it is important to note that only a small number and narrow variety of MOF membranes have been fabricated and examined for H_2/N_2 separation to date. Considering the large number of available MOFs and the continuous growth in the synthesis of new materials, many MOFs having high H_2/N_2 selectivities and high H_2 permeabilities possibly exist. Fabrication of membranes from every single synthesized MOF material and experimental measurement of their H_2/N_2 separation performances are not practical due to the significant time and resource requirements of membrane synthesis from new materials.

High-throughput computational screening methods play a crucial role in efficiently examining large numbers of materials to identify the best candidates for a gas separation of interest. Large-scale computational screening studies using molecular simulation techniques have been performed to find the top MOF adsorbents having high selectivities specifically for CO_2 separations.[22−24] However, a similar type of computational screening study has not been extensively performed for MOF membranes due to the computational expense and long time necessity of modeling gas transport through membranes. A few studies focused on the computational screening of MOF membranes for different gas separations such as CO_2/CH_4, CO_2/H_2, CO_2/N_2, and He/CH_4. For example, Watanabe and Sholl[25] screened 1163 MOFs as membrane materials for CO_2/N_2 separation and proposed the 10 best MOFs based on their selectivities computed at infinite dilution at 303 K. Jiang and coworkers[26] performed a computational study to screen 137 953 hypothetical (computer-generated) MOF membranes at infinite dilution and selected the top 24 MOF membranes for further investigation at 10 bar and 298 K for binary CO_2/CH_4 and ternary $CO_2/N_2/CH_4$ mixture separations. In their following study,[27] they examined 4764 computation-ready experimental MOFs for separation of ternary $CO_2/N_2/CH_4$ gas mixtures at 10 bar and 298 K and proposed the 7 best MOF membranes with the highest CO_2/CH_4 and N_2/CH_4 selectivities. Wilmer and coworkers[28] recently screened both the synthesized and hypothetical MOFs to predict CO_2/N_2 separation performances of mixed matrix membranes (MMMs) composed of MOFs. Our group identified several top-performing MOF membranes for H_2/CH_4,[29] He/CH_4,[30] CO_2/CH_4,[31] CO_2/H_2,[32] and CO_2/N_2[33] separations by screening large numbers of materials using molecular simulations. As this literature review summarizes, none of the large-scale computational screening studies focused on MOF membranes for H_2/N_2 separation to date and the knowledge about H_2/N_2 separation potential of MOF membranes and MOF-based MMMs is currently very limited in the literature.

Motivated from this, we investigated membrane-based H_2/N_2 separation performances of MOFs combining grand canonical Monte Carlo (GCMC) and molecular dynamics (MD) simulations. We first computed H_2 and N_2 permeabilities and ideal H_2/N_2 selectivities of 3765 MOF membranes at infinite dilution at room temperature. MOF membranes that can exceed the Robeson's upper bound,[3] which was established for polymeric membranes, were identified, and the top 20 MOFs were selected based on their H_2/N_2 selectivities. In the next step, molecular simulations were performed for these top membranes considering binary H_2/N_2:30/70 and quaternary $H_2/N_2/CO_2/CO$:16.4/60.5/5.3/17.9 mixtures to assess the gas separation performances of MOFs under practical operating conditions, 1 bar and 298 K. Gas permeabilities and selectivities obtained at infinite dilution; binary mixture and quaternary mixture conditions were compared to understand the multicomponent mixture effects on the predicted gas separation performances of MOF membranes. Structural properties of MOFs such as pore sizes, pore volumes, surface areas, and lattice types were also described, and their correlations with H_2/N_2 separation performances of MOF membranes were investigated to gain molecular-level insights into the optimum structural properties of the best MOF membranes which can accelerate the design and development of new MOFs with outstanding H_2/N_2 separation potentials. Finally, we examined MOF/polymer MMMs where the top MOFs obtained from our high-throughput screening approach were used as fillers in six different polymers that are close to the upper bound. H_2 permeabilities, N_2 permeabilities, and H_2/N_2 selectivities of MOF-based MMMs were computed to assess the contribution of MOFs in enhancing the separation performance of the polymer membranes. Results of this study will be beneficial to guide the future experimental work in this field by unlocking the potentials of pristine MOF membranes and MOF-based polymer membranes in H_2/N_2 separations.

SIMULATION DETAILS

We computationally screened the most recent MOF subset of the Cambridge Structural Database (CSD) which contains 54 808 nondisordered MOFs.[34] To mimic the experimental activation procedure of MOFs, we removed the solvent molecules using the publicly available Python script[34] to make the MOFs' pores available for the adsorption and transport of gas molecules. Structural properties such as the largest cavity diameter (LCD), pore limiting diameter (PLD), accessible gravimetric surface area (SA), and pore volume of MOFs were calculated using the Zeo++ software.[35] Probe sizes of 3.6 Å (kinetic diameter of N_2 molecule) and 0 Å were used for the calculation of SA and pore volume, respectively. We only considered the MOFs having SA > 0 m^2/g and PLD > 3.75 Å so that both H_2 and N_2 gases can permeate through the MOF membranes'

DOI: 10.1021/acssuschemeng.9b01020
ACS Sustainable Chem. Eng. 2019, 7, 9525−9536

Table 1. Calculated Properties of MOF Membranes[a]

		formula
infinite dilution condition	permeability (Barrer)	$P_i^0 = K_i^0 \times D_i^0$
	adsorption selectivity	$S^0_{ads,H_2/N_2} = \frac{K^0_{H_2}}{K^0_{N_2}}$
	diffusion selectivity	$S^0_{diff,H_2/N_2} = \frac{D^0_{H_2}}{D^0_{N_2}}$
	membrane selectivity	$S^0_{mem,H_2/N_2} = S^0_{ads,H_2/N_2} \times S^0_{diff,H_2/N_2}$
binary (B) and quaternary (Q) mixture conditions	permeability (Barrer)	$P_i^{B(Q)} = \frac{N_i^{B(Q)} \times D_i^{B(Q)}}{f_i}$
	adsorption selectivity	$S^{B(Q)}_{ads,H_2/N_2} = \frac{N_{H_2}}{N_{N_2}} \Big/ \frac{y_{H_2}}{y_{N_2}}$
	diffusion selectivity	$S^{B(Q)}_{diff,H_2/N_2} = \frac{D^{B(Q)}_{H_2}}{D^{B(Q)}_{N_2}}$
	membrane selectivity	$S^{B(Q)}_{mem,H_2/N_2} = S^{B(Q)}_{ads,H_2/N_2} \times S^{B(Q)}_{diff,H_2/N_2}$
MMM calculations	permeability (Barrer)	$P_{MMM} = P_p \times \frac{n\times P_{MOF} + (1-n)\times P_p - (1-n)\times \phi \times (P_p - P_{MOF})}{n\times P_{MOF} + (1-n)\times P_p + n\times \phi \times (P_p - P_{MOF})}$

[a] i: gas species, H_2 or N_2; K_i^0: Henry's constant at infinite dilution (mol/kg/Pa); D_i^0: self-diffusivity at infinite dilution (cm^2/s); f: partial pressure of gas in the mixture (Pa); N: gas uptake at mixture condition (mol/kg); y: molar fraction of gas species in the mixture; P_{MMM}: gas permeability of MOF/polymer MMM (Barrer); P_p: gas permeability of polymer (Barrer); P_{MOF}: gas permeability of MOF (Barrer); n: geometry shape factor; ϕ: volume fraction of MOF filler in MMM; 1 Barrer = 3.348×10^{-16} mol m/(m^2 s Pa).

pores. After these refinements, we ended up with 3765 materials representing a wide range of structural and chemical properties.

GCMC and MD simulations were performed using the RASPA simulation software.[36] Adsorption and diffusion of gases were examined at three different conditions in this work: (i) for single-component H_2 and N_2 at infinite dilution, (ii) for binary H_2/N_2 mixture, and (iii) for quaternary $H_2/N_2/CO_2/CO$ mixture. Intermolecular interactions were defined using the Lennard–Jones (LJ) potential, and the Lorentz–Berthelot mixing rule was applied to parametrize the effective pair potentials. The potential parameters of MOFs were taken from the Universal Force Field (UFF)[37] because UFF is applicable to all MOFs having various types of atoms.[38] MOFs were assumed to be rigid in molecular simulations to save significant computational time. The cutoff radius was set to 13 Å, and the length of unit cells of MOFs in each dimension was expanded to at least 26 Å. Besides LJ interactions, electrostatic interactions were also considered for N_2, CO, and CO_2 molecules using the Coulomb potential, and these interactions were evaluated using the Ewald summation. Partial point charges were assigned to MOF atoms using the charge equilibrium method (QEq)[39,40] as implemented in the RASPA to calculate the electrostatic interactions between adsorbates and MOF atoms. N_2 was modeled as a three-site rigid molecule where two sites were N atoms and the other site was the center of mass with partial point charges.[41] Single-site spherical model with LJ 12-6 potentials was used for H_2.[42] We showed the good agreement between experiments and simulations using this model for adsorption isotherms of H_2 in several MOFs, including Cu-BTC, ZIF-8, and IRMOF-1 at a wide range of pressures.[43] We modeled H_2 as nonpolar in our simulations; therefore, there was no electrostatic interaction between H_2 and MOFs. H_2 has a nonzero quadrupole moment, but charge–quadrupole interactions between Cu-BTC and adsorbed H_2 molecules were found to be negligible at 298 K.[44] A three-site model was used for CO which was provided by Fisher et al.[45] where LJ parameters were adapted from Gu et al.[46] and the point charges were adapted from Straub and Karplus models.[47] CO_2 was represented as a three-site rigid model with partial point charges located at the center of each site.[48] The potentials used for gas molecules are given in Table S1 of Supporting Information.

We first computed the Henry's constants (K_i^0) and self-diffusion coefficients (D_i^0) of the single-component gases (i), H_2 and N_2, at infinite dilution for 3765 MOFs. The Widom particle insertion method was used with 5000 initialization cycles and 10 000 production cycles to calculate K_i^0 values at 298 K. Thirty adsorbate molecules were inserted into each MOF to calculate the self-diffusivities of gas molecules, D_i^0, using MD approach, and intermolecular interactions were omitted between the gas molecules to imitate the infinite dilution condition. NVT ensemble with Nose–Hoover thermostat[49] was used, and the number of cycles was set to 1000 for initialization, 10^4 for equilibration, and 10^6 for production. D_i^0 values for each gas molecule were calculated using the slope of the mean square displacement obtained from the MD simulations. Using the data of K_i^0 and D_i^0, gas permeability (P_i^0), adsorption selectivity ($S^0_{ads,H_2/N_2}$), diffusion selectivity ($S^0_{diff,H_2/N_2}$), and membrane selectivity ($S^0_{mem,H_2/N_2}$) were calculated for each MOF at infinite dilution as shown in the equations given in Table 1. All selectivities were computed for H_2 over N_2. We identified MOFs exceeding the upper bound and focused on the top 20 MOF membranes exhibiting the highest selectivities.

In the next step, we examined mixture separation performances of the top 20 MOF membranes identified from the molecular simulations performed at infinite dilution. Molecular simulations were performed for the top MOF membranes considering binary H_2/N_2:30/70[50] and quaternary $H_2/N_2/CO_2/CO$:16.4/60.5/5.3/17.9[2] mixtures for which compositions were taken from the literature. Molecular simulations were done at 1 bar and 298 K to assess the real gas separation performances of MOFs under practical operating conditions. Adsorbate–adsorbate and adsorbate–MOF interactions were considered in the mixture simulations. GCMC simulations with 20 000 initialization and 100 000 production cycles were performed to compute the adsorbed gas loadings of the binary and quaternary mixtures, and MD simulations with 5000 initialization cycles were performed using these calculated gas loadings to compute the self-diffusivities of each gas component in the mixtures. Adsorption and diffusion data were then combined as shown in the equations given in Table 1 to compute gas permeability (P_i^B), adsorption selectivity ($S^B_{ads,H_2/N_2}$), diffusion selectivity ($S^B_{diff,H_2/N_2}$), and membrane selectivity

DOI: 10.1021/acssuschemeng.9b01020
ACS Sustainable Chem. Eng. 2019, 7, 9525–9536

($S^{B}_{mem,H_2/N_2}$) of each MOF membrane for separation of binary H_2/N_2:30/70 mixture. Similarly, quaternary $H_2/N_2/CO_2/CO$:16.4/60.5/5.3/17.9 mixture separation performances of MOF membranes were estimated by computing gas permeability (P_i^Q), adsorption selectivity ($S^{Q}_{ads,H_2/N_2}$), diffusion selectivity ($S^{Q}_{diff,H_2/N_2}$), and membrane selectivity ($S^{Q}_{mem,H_2/N_2}$) of each MOF membrane.

At the final step, we examined H_2/N_2 separation performances of MOF-based polymer membranes. The top MOFs were considered as fillers, and six different types of polymers were considered as continuous phases of MOF/polymer MMMs. The polymers that are close to the Robeson's upper bound for H_2/N_2 separation were selected.[3] These are polybenzoxazinone imide (PBOI-2-Cu$^+$),[51] cross-linked *N,N′*-dipropargyl (4−4′-hexafluoroisopropylidene) bisphthalimide polyimide (6FDA-DIA),[52] protonated form of 1,4,5,8-naphthalene tetracarboxylic dianhydride-2,2-bis[4-(4-aminophenoxy)-phenyl] hexafluoro propane disulfonic acid polyimide (NTDA-BAPHFDS(H)),[53] polymer of intrinsic microporosity-7 (PIM-7),[54] PIM-1,[54] and poly(trimethylsilyl propyne) (PTMSP).[55] Experimentally reported H_2 permeabilities, N_2 permeabilities, and ideal H_2/N_2 selectivities of these polymeric membranes were obtained from the literature and given in Table S2. We previously showed the good agreement between the experimental measurements and theoretical predictions of the Maxwell model[56] for H_2 permeabilities of several MOF-based MMMs such as IRMOF-1/Matrimid, Cu-BTC/polysulfone, Cu-BTC/polydimethylsiloxane (PDMS), and N_2 permeabilities of Cu-BTC/polyimide, ZIF-8/Matrimid, ZIF-8/Ultem, and ZIF-8/poly(1,4-phenylene ether-ether-sulfone (PPEES) MMMs.[57,58] Motivated from these works, permeabilities of MOF-based MMMs (P_{MMM}) were computed using the Maxwell model given in Table 1. The Maxwell model was developed to predict the effective permeability of gases through the MMMs using the gas permeability data of polymer matrix and filler particles. Its main assumption is that the contact between two phases at the polymer−particle interface is defect-free, and the model considers a diluted suspension of spherical particles with low filler concentration.[56] The geometry shape factor (n) was taken as 0.3 assuming sphere-like MOF particles; the volume fraction of the MOFs in MMMs (ϕ) was used as 0.2.[59] P_{MOF} in this model represents the gas permeability of MOF calculated from the results of GCMC and MD simulations, which were carried out exactly at the same pressure and temperature with the gas permeability measurements of polymeric membranes (P_P) as reported in Table S2.

RESULTS AND DISCUSSION

In our previous studies,[29,60] we validated the accuracy of our computational approach by comparing the experimentally reported single-component H_2 and N_2 permeabilities of various types of MOF membranes with the predictions of molecular simulations. In this work, we additionally compared results of our molecular simulations for H_2/N_2 mixture permeances of several MOF membranes with the available experimental data under the same conditions. Since most of the experimental work reported gas permeances of MOF membranes, we converted our simulated permeabilities to permeances using the membrane thickness values given in Table S3 to compare simulation results with the experiments. Details about the experimental conditions of gas permeance measurements of MOF membranes are also given in Table S3. Figure 1 shows that simulation results for single-component H_2 and N_2 permeances through Ni-MOF-74 and MOF-5 membranes and H_2/N_2 mixture permeances through ZIF-22, ZIF-78, and ZIF-90 membranes agree well with experimental data. This good agreement between simulations and experiments indicates that molecular simulations that we described above can be used to accurately estimate H_2/N_2 permeation through MOF membranes. Motivated from this, we computed H_2 and

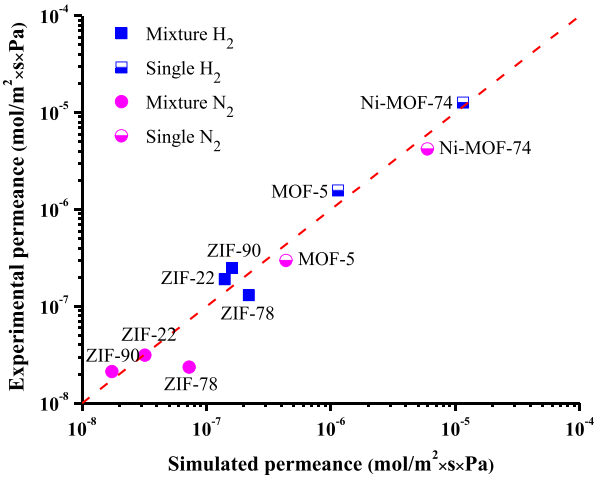


Figure 1. Comparison of the experimental[7,20,71−73] and simulated H_2 and N_2 permeances of MOF membranes. Details of the experimental data are given in Table S3. Diagonal line is to guide the eye.

N_2 permeabilities of 3765 MOFs that have not been experimentally tested for membrane-based H_2/N_2 separations.

For an efficient membrane-based gas separation process, high gas permeability and high selectivity are desired. It is well-known that there is a trade-off between permeability and selectivity of polymeric membranes; membranes having high H_2 permeability suffer from low H_2 selectivity and vice versa. To show this trade-off, Robeson[3] defined an upper bound for the performance of polymeric membranes for H_2/N_2 separation. The upper bound correlation was defined based on the single-component gas permeability measurements of polymeric membranes which rely on the solution/diffusion transport rather than molecular sieving effect. We showed H_2 permeabilities and ideal H_2/N_2 selectivities of 3765 MOF membranes computed at infinite dilution at 298 K in Figure 2 together with the upper bound of polymers. Our results showed that the trade-off between the gas permeability and selectivity of polymeric membranes is not valid for MOF

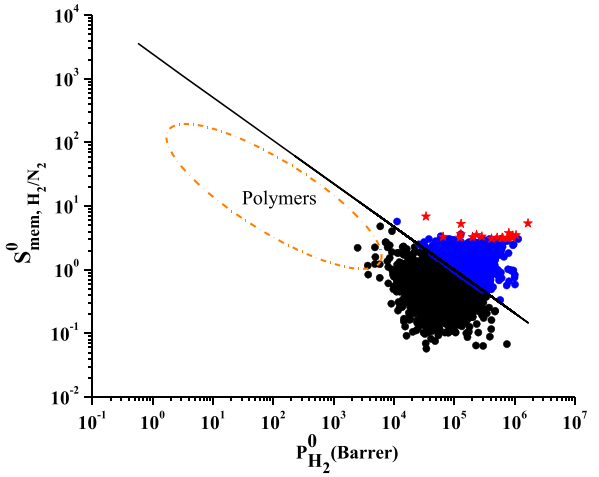


Figure 2. H_2 permeability and H_2/N_2 selectivity of MOF membranes calculated at infinite dilution. The black solid line represents the Robeson's upper bound for polymeric membranes. Black and blue points represent MOFs which are under and above the Robeson's bound, respectively. Red stars represent the top 20 MOF membrane candidates.

DOI: 10.1021/acssuschemeng.9b01020
ACS Sustainable Chem. Eng. 2019, 7, 9525−9536

membranes because many MOFs are able to exceed the upper bound. Polymeric membranes generally exhibit high H_2/N_2 selectivities between 2 and 300 but low H_2 permeabilities varying in the range of $1-10^4$ Barrer. Permeabilities of MOF membranes were computed to be in the range of 2.5×10^3 to 1.7×10^6 Barrer, whereas their H_2/N_2 membrane selectivities were calculated to be between 0.06 and 6.9. Although all the MOF membranes we examined in this study were found to have lower H_2/N_2 selectivities than the polymeric membranes, H_2 permeabilities of MOF membranes are drastically larger than those of polymers, which can be attributed to high porosities of MOFs. Because of high porosities, both H_2 and N_2 can easily penetrate through the MOF membranes' pores, leading to lower selectivities compared to those of polymers. One thousand three hundred and fifty-one MOFs were found to exceed the Robeson's upper bound due to their high H_2 permeabilities ranging from 1.1×10^4 to 1.7×10^6 Barrer. We ranked the MOF membranes based on their H_2/N_2 selectivities from the highest to the lowest, and the top 20 MOFs were identified, as shown by red stars in Figure 2. We note that KA, NaA, and CaA zeolite membranes were reported to exhibit moderate H_2 permeabilities, 1.3×10^3 to 2.7×10^3 Barrers, and H_2/N_2 selectivities between 5.9 and 9.9.[61] H_2/N_2 selectivities of MFI-type zeolite and SSZ-13 membranes were reported as 1.5–4.5 and 4–5, respectively.[62,63] Pd-based membranes have been reported to have H_2 permeabilities of 10^3 to 1.3×10^4 Barrer and very high H_2 selectivities, even reaching 2000 at very high temperatures of 400–600 °C.[4] Because operating membranes at high temperatures is not economical, MOFs can be alternatives to polymer, zeolite, and metal membranes for H_2/N_2 separations by offering a good combination of high H_2 permeabilities and moderate H_2 selectivities at room temperatures.

We examined adsorption and diffusion selectivities to understand their contributions into H_2/N_2 separation mechanisms of MOF membranes. In Figure 3(a), membrane selectivity was compared with the adsorption selectivity for 3765 MOFs. One thousand three hundred and fifty-one promising MOFs that exceed the upper bound and the top 20 MOFs that we identified are shown by blue and red symbols, respectively, in Figure 3(a). All the MOFs have $S^0_{ads,H_2/N_2} < 1$, meaning that MOFs are N_2 selective in adsorption process. This can be explained by the very weak interaction of H_2 with the MOF atoms and additional electrostatic interactions of N_2 with the MOF atoms. Although all MOFs prefer N_2 over H_2 in adsorption, 1304 MOFs were found to selectively separate H_2 from N_2 ($S^0_{mem,H_2/N_2} > 1$) in membrane-based separation, as shown in Figure 3(a), indicating the dominant effect of diffusion. Diffusion selectivity favors H_2 over N_2 because lighter and smaller H_2 (kinetic diameters of H_2: 2.89 Å, N_2: 3.64 Å) diffuses faster than N_2, which leads to $S^0_{diff,H_2/N_2}$ values greater than 1 for all MOFs, ranging from 1.5 to 147. As a result, selective separation of H_2 from N_2 occurs when the diffusion selectivity of MOF toward H_2 dominates the adsorption selectivity of MOF toward N_2. We color-coded the diffusion selectivities of 1351 MOFs exceeding the upper bound in Figure 3(b). MOFs exceeding the upper bound have $S^0_{ads,H_2/N_2}$ and $S^0_{diff,H_2/N_2}$ values in the ranges of 0.02–0.7 and 3–147, respectively. MOFs with high $S^0_{ads,H_2/N_2}$ (0.3–0.7) generally have low $S^0_{diff,H_2/N_2}$ (2–10) and vice versa. Higher adsorption selectivity means more gas molecules interact with

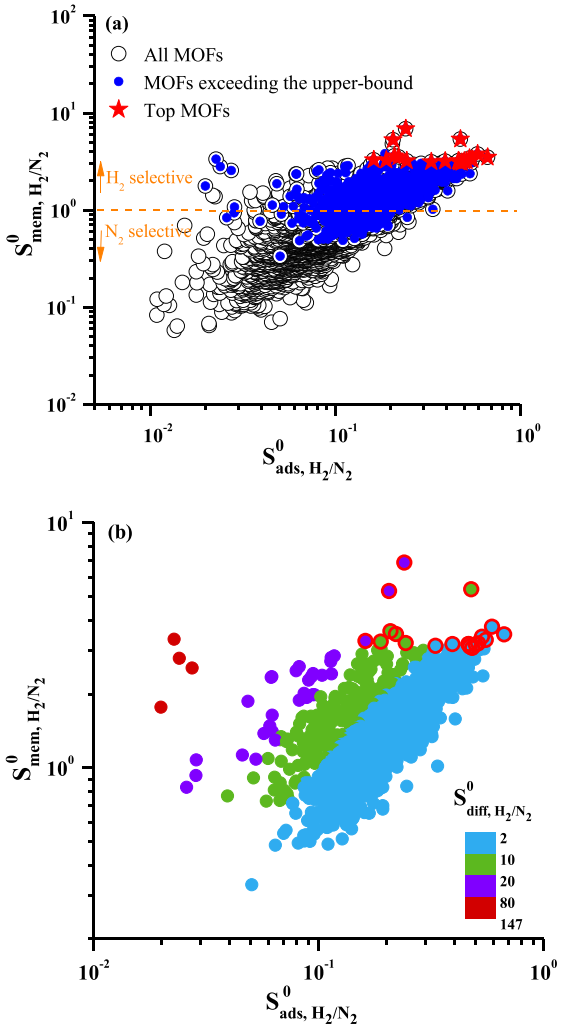


Figure 3. (a) Comparison of membrane and adsorption selectivity of MOFs computed at infinite dilution. Black and blue points represent all MOFs and MOFs exceeding the upper bound, respectively. Red starts represent the top 20 MOFs identified in this work. The dashed line shows the gas preference of the MOF membrane. (b) Comparison of membrane, adsorption, and diffusion selectivity of MOFs exceeding the upper bound. The top 20 MOFs are shown with red borders.

the framework and accumulate inside the pores, which decreases the gas diffusion rates due to the steric hindrance. As a result, materials having high adsorption selectivity for a gas molecule (N_2 for all MOFs) suffer from the low diffusion selectivity toward the same molecule. As we discussed above, the top 20 MOFs were selected based on $S^0_{mem,H_2/N_2}$ values which consider both $S^0_{ads,H_2/N_2}$ and $S^0_{diff,H_2/N_2}$ and these best membrane candidates were computed to have $S^0_{ads,H_2/N_2}$ values of 0.2–0.7 and $S^0_{diff,H_2/N_2}$ values of 5–28.5. This result highlights the pronounced effect of diffusion on the membrane-based separation performances of MOFs.

In the first step, we performed all molecular simulations of MOFs at infinite dilution for the computational efficiency of the screening process. Once the top 20 MOF membrane candidates were identified, computationally demanding binary and quaternary mixture simulations were carried out to unlock the membrane performance of the best MOFs under practical operating conditions in the second step. Permeability and

DOI: 10.1021/acssuschemeng.9b01020
ACS Sustainable Chem. Eng. 2019, 7, 9525–9536

selectivity of MOF membranes were computed considering a binary gas mixture of H_2/N_2:30/70 and a quaternary mixture of $H_2/N_2/CO_2/CO$:16.4/60.5/5.3/17.9 at 1 bar and 298 K. Figure 4 represents the comparison of predicted separation

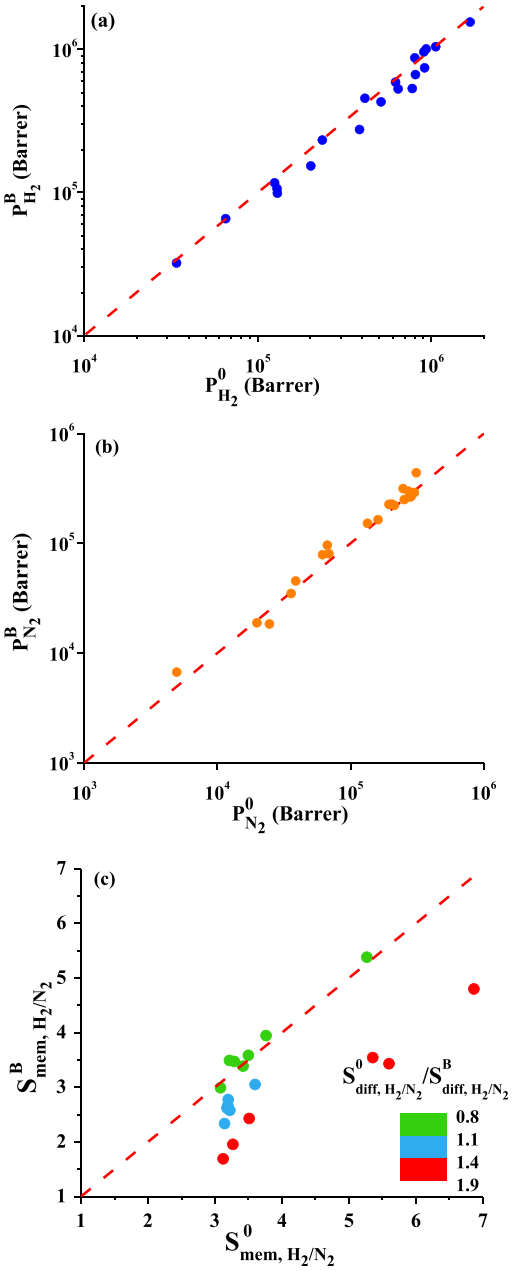


Figure 4. Comparison of (a) H_2 permeability, (b) N_2 permeability, and (c) H_2/N_2 selectivity of the top 20 MOF membranes computed at infinite dilution and at binary mixture conditions. The diagonal dashed lines are given to guide the eye.

performances of the top MOFs at binary mixture and infinite dilution conditions. Figures 4(a) and (b) show that MOFs generally have slightly lower H_2 and higher N_2 permeabilities at binary mixture conditions compared to the infinite dilution. While H_2 molecules in the mixture rapidly diffuse through the membrane, they speed up the bulky and slow N_2 molecules. In the opposite way, existence of the bulky and slow diffusing N_2 molecules in the feed mixture decreases the diffusion rate of H_2 molecules. As a result, lower H_2 and higher N_2 permeabilities were predicted at binary mixture conditions, and H_2/N_2 selectivities of MOF membranes were slightly lower in the mixture case compared to the ones obtained at the infinite dilution, as shown in Figure 4(c). Adsorption selectivities of MOFs at infinite dilution (0.16−0.67) were computed to be very similar to the ones obtained at binary mixture case (0.15−0.68). Therefore, we focused on the effect of diffusion selectivity on the membrane performance and color-coded the MOFs in Figure 4(c) based on the ratio of diffusion selectivity computed at infinite dilution to the one computed at binary mixture condition (S^0_{diff}/S^B_{diff}). Green symbols show the MOFs with similar S^0_{diff} and S^B_{diff} values resulting in S^0_{diff}/S^B_{diff} values between 0.8 and 1.1. Because both adsorption selectivity and diffusion selectivity computed at infinite dilution and binary mixture condition are similar, these are the MOFs predicted to have almost the same membrane selectivities under two different conditions. As the S^0_{diff}/S^B_{diff} ratio deviates from unity, the difference between S^0_{mem} and S^B_{mem} becomes more pronounced. For example, 6 MOFs among the top 20 MOFs have S^0_{diff}/S^B_{diff} values between 1.4 and 1.9 as presented by red symbols in Figure 4(c). S^0_{mem} values of these MOFs are almost twice their S^B_{mem} values, highlighting the dominant effect of the diffusion selectivity on the membrane performance of MOFs. We note that membrane selectivities computed at infinite dilution (3.1−6.9) generally well estimated the ones computed at binary mixture conditions (1.7−5.4), indicating that performing molecular simulations initially at infinite dilution can be an efficient screening approach for identifying the most selective membranes for separation of binary H_2/N_2 mixtures.

Similarly, we compared permeabilities and selectivities of the top 20 MOF membranes at binary and quaternary mixture conditions at 1 bar and 298 K. H_2 and N_2 permeabilities were calculated as well as H_2/N_2 membrane selectivities for the separation of quaternary $H_2/N_2/CO_2/CO$ mixtures. Figure 5 shows that performances of MOF membranes for separation of binary and quaternary mixtures are quite similar. For most of the MOF membranes, binary mixture permeabilities were found to be slightly larger than the quaternary mixture permeabilities, which were attributed to the presence of other polar molecules, CO_2 and CO, in the quaternary mixture that hinder the transport of N_2 and H_2 gases. Comparison of the membrane selectivities at the binary and quaternary mixture conditions shown in Figure 5(c) restated the effect of diffusion selectivity as we discussed above. Because adsorption selectivities at the conditions of binary (0.15−0.68) and quaternary mixtures (0.15−0.66) were computed to be almost the same, MOFs having similar diffusion selectivities in the binary and quaternary mixture conditions ($0.9 < S^B_{diff}/S^Q_{diff} < 1.1$) exhibit similar membrane selectivities. On the other hand, MOFs that have larger (smaller) diffusion selectivities in the binary mixture compared to the quaternary mixture, $1.1 < S^B_{diff}/S^Q_{diff} < 1.4$ ($0.7 < S^B_{diff}/S^Q_{diff} < 0.9$), were found to overpredict (underpredict) the membrane selectivities at the quaternary mixture condition. Because performing binary mixture simulations is computationally much easier than performing the same simulations for a quaternary mixture, binary mixture simulations can be safely used to estimate $H_2/N_2/CO_2/CO$ mixture separation performance of MOF membranes.

Gas permeabilities and selectivities of the top 20 MOF membranes at infinite dilution and binary and quaternary mixture conditions are given in Table 2. H_2 permeabilities were computed as $3.4 \times 10^4 < P^0_{H_2} < 1.7 \times 10^6$, $3.2 \times 10^4 < P^B_{H_2} < 1.6$

DOI: 10.1021/acssuschemeng.9b01020
ACS Sustainable Chem. Eng. 2019, 7, 9525−9536

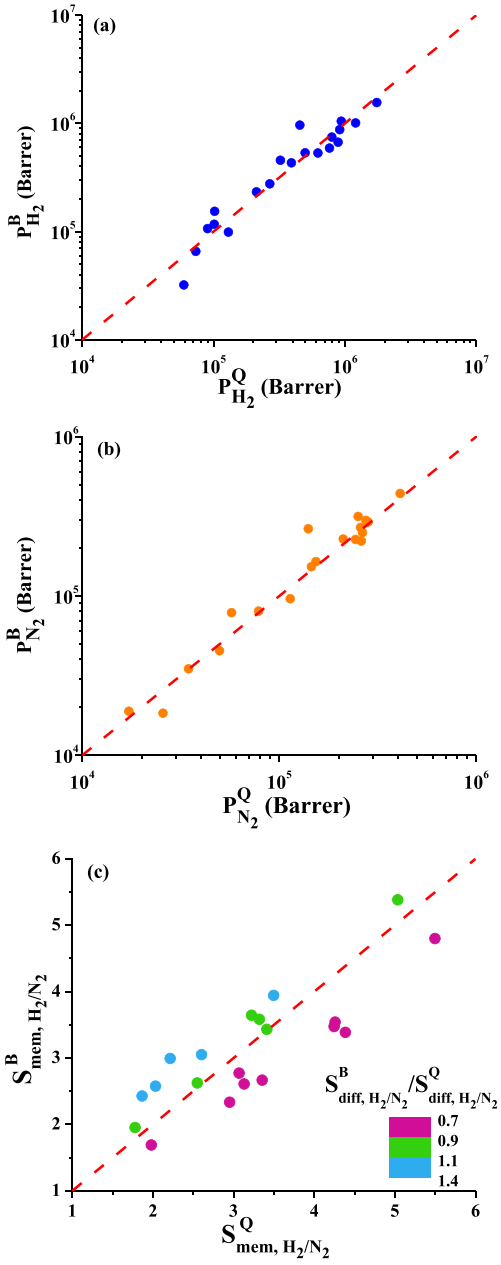


Figure 5. Comparison of (a) H_2 permeability, (b) N_2 permeability, and (c) H_2/N_2 selectivity of the top 20 MOF membranes computed at binary and quaternary mixture conditions. The diagonal dashed lines are given to guide the eye.

$\times 10^6$, and $5.9 \times 10^4 < P^Q_{H_2} < 1.8 \times 10^6$ Barrer at infinite dilution and binary and quaternary mixture conditions, respectively. N_2 permeabilities were calculated to be much lower at $4.9 \times 10^3 < P^0_{N_2} < 3.1 \times 10^5$, $6.7 \times 10^3 < P^B_{N_2}$ 4.4×10^5, and $1.1 \times 10^4 < P^Q_{N_2} < 4.1 \times 10^5$ Barrer. FOTNIN has the highest H_2 and N_2 permeabilities which can be attributed to its large PLD (28.5 Å) and LCD (33.6 Å), leading to high gas diffusivities. Selectivities of the top membranes were similar under different conditions, $3.1 < S^0_{mem,H_2/N_2} < 6.9$, $1.7 < S^B_{mem,H_2/N_2} < 5.4$, and $1.8 < S^Q_{mem,H_2/N_2} < 5.5$. The highest membrane selectivities at infinite dilution and quaternary mixture conditions belong to GUPCUQ01, a cadmium imidazolate framework (CdIF-8), which was synthesized as the replacement of Zn in ZIFs with Cd.[64] As we discussed in the beginning, ZIF membranes exhibited the highest H_2/N_2 selectivities among the fabricated MOF membranes. The PLD (3.83 Å) and LCD (12.6 Å) of GUPCUQ01 were computed to be comparably smaller than the other top membranes, enhancing the selective separation of H_2 from N_2. This MOF exhibits one of the highest H_2/N_2 diffusion selectivities among the top membranes at all three conditions (28.5, 20, and 22.5 at infinite dilution, binary and quaternary mixture conditions, respectively) with moderate adsorption selectivities (0.24 at all conditions), leading to high membrane selectivities.

Analysis of a large number of MOFs assists to reveal the structure−performance relations, which provides valuable information to guide the experimentalists on synthesizing new MOFs with better membrane performances. We computed the structural properties of all MOFs such as PLD, LCD, SA, and pore volume and listed them in Table S4. We also described the lattice types of MOFs using the information given in crystal structure files provided in the Cambridge Crystallographic Data Centre (CCDC).[65] Figure 6 shows structure−performance relations for all MOFs, for MOFs that are able to exceed the upper bound, for the top 20 and top 10 MOF membranes. Our analysis showed that although significant numbers of MOFs, 2661, have PLDs between 3.75 and 6 Å, only 3 MOFs appeared in the top 10 material list. A small number of MOFs, 88 among 3765, have large PLDs (>12 Å), and 5 of them were in the top 10 list. A similar trend is valid for LCD−performance relation. MOFs with LCDs in the range of 4.2−7 Å are 57% of the materials we considered; however, none of them is among the top MOFs and 17 (9) out of the top 20 (10) MOFs have LCDs > 12 Å. These results show that MOFs with large pore sizes (PLD > 6 Å and LCD > 12 Å) are promising for H_2/N_2 separation, in agreement with the literature because a similar conclusion was drawn for the best MOF membranes for H_2/CO_2 separation.[32] Almost half of the studied MOFs have SA < 1000 m^2/g, only one of them is present among the top 20 membranes. Three of the top 10 membranes have SA > 3500 m^2/g. Among the top 20 (10) MOFs, 13 (5) of them have pore volumes >1 cm^3/g. Three thousand seven hundred and sixty-five MOFs considered in this work were categorized in eight different lattice types, and the top MOFs had only four different lattice types: cubic, hexagonal, orthorhombic, and rhombohedral. A significant number of MOFs, 1445 among 3765, was monoclinic, but none of the top materials has this lattice type. Overall, according to Figure 6, the most promising MOF membranes for H_2/N_2 separation are generally cubic with large PLDs (>6 Å) and LCDs (>12 Å) as well as high surface areas (3500 m^2/g) and high pore volumes (>1 cm^3/g).

Other than the structural properties, we also examined the experimental synthesis papers of the top MOF candidates to get information about their stabilities. As explained in the beginning, we screened the MOF database integrated with the CSD and simulated solvent-free MOFs by removing the solvents using the Python script provided in the MOF database.[34] Automated removal of solvents is performed in high-throughput MOF screening studies to mimic experimentally activated structures but in some cases it may affect the framework integrity and/or stability. However, it is simply not practical to check several thousands of MOFs one by one to see if the solvent removal would cause a stability problem. We only analyzed the top MOFs to ensure that automatic solvent removal process does not cause a structural stability problem.

DOI: 10.1021/acssuschemeng.9b01020
ACS Sustainable Chem. Eng. 2019, 7, 9525−9536

Table 2. Performances of the Top 20 MOF Membranes Computed at Infinite Dilution, Binary and Quaternary Mixture Conditions[a]

MOF	S^0_{mem}	S^B_{mem}	S^Q_{mem}	$P^0_{H_2} \times 10^4$ (Barrer)	$P^B_{H_2} \times 10^4$ (Barrer)	$P^Q_{H_2} \times 10^4$ (Barrer)	$P^0_{N_2} \times 10^4$ (Barrer)	$P^B_{N_2} \times 10^4$ (Barrer)	$P^Q_{N_2} \times 10^4$ (Barrer)
BEDYEQ	3.14	2.33	2.95	64.29	53.01	62.30	20.45	22.71	21.11
ECOKAJ	3.42	3.38	4.39	93.40	100.74	120.68	27.29	29.77	27.51
FOTNIN	5.36	3.54	4.26	167.02	155.36	174.97	31.18	43.88	41.08
GESVAC	3.08	2.99	2.22	41.44	45.57	32.24	13.43	15.24	14.55
GULWEQ	3.51	2.43	1.87	23.53	23.26	21.24	6.70	9.59	11.38
GUPCUQ01	6.86	4.80	5.50	3.40	3.21	5.95	0.50	0.67	1.08
HEXVEM	3.22	3.49	3.22	90.50	96.03	45.31	28.13	27.40	14.05
IZOWAW	5.60	3.43	3.41	38.51	27.55	26.85	6.88	8.04	7.87
MEGBEH	3.22	2.57	2.03	12.48	11.66	10.13	3.87	4.53	4.98
MOVPOE	5.27	5.38	5.04	12.96	9.87	12.96	2.46	1.83	2.57
PIBPIA	3.12	1.69	1.98	77.57	53.27	49.82	24.84	31.51	25.13
PUGPEO	3.27	1.95	1.78	20.17	15.33	10.19	6.17	7.85	5.72
RUBDUP	3.20	2.77	3.07	91.33	74.43	79.40	28.54	26.85	25.86
RUBTAK02	3.29	3.47	4.25	6.53	6.55	7.34	1.98	1.89	1.73
SIZPUN	3.60	3.05	2.60	12.89	10.63	9.02	3.58	3.49	3.46
TOCJAY	3.19	2.67	3.36	80.84	66.67	88.70	25.32	25.00	26.43
TURFIX	3.76	3.94	3.50	80.37	87.21	91.14	21.35	22.12	26.06
VAGMAT	3.19	2.61	3.13	62.08	59.00	76.41	19.46	22.62	24.41
XANLEF	3.18	2.62	2.55	51.24	43.00	39.20	16.10	16.39	15.37
XANLIJ	3.50	3.58	3.32	105.86	104.22	93.81	30.23	29.11	28.24

[a]Membrane selectivities were reported for H_2 over N_2.

To investigate the top MOFs in detail, we referred to the original experimental synthesis studies of the top 20 materials and inferred that 5 MOFs might suffer from the thermal stability problems once their solvents are removed as explained in detail in Table S5. Our careful comparison between crystal structures reported in the CSD and the corresponding experimental structures reported in the synthesis papers also showed that 9 of the top 20 have some structural issues because of the way they were deposited into the CSD.[65] More specifically, four MOF structures were found to be deposited into the CSD with missing hydrogen atoms; three MOFs were deposited with disordered coordinated solvent molecules, and one structure was missing charge balancing ions, the other was missing functional groups attached to the ligands, as explained in detail in Table S5. We edited four MOFs (GESVAC, RUBTAK02, XANLEF, and XANLIJ) by adding missing hydrogen atoms using Mercury software[66] and manually removed the disordered solvent molecules of three MOFs (BEDYEQ, FOTNIN, and SIZPUN), which were not recognized as solvent by the Python script due to the disordered atoms. We then repeated the GCMC simulations for adsorption and diffusion of binary H_2/N_2 mixtures in these 7 edited MOFs. Results given in Table S6 show that simulated H_2 permeabilities of the edited MOFs were even higher than those of the CSD-deposited structures that we used from the MOF database[34] except one structure. Selectivities of the edited MOFs were also in the same range (1.5−9.6) with those of the original structures (2.3−3.6), indicating that these MOFs are still promising (in some cases even more promising) membrane materials. After discarding 5 MOFs that may have stability problems and 2 MOFs with missing functional groups and charge balancing ions, we proceeded with 13 promising MOFs which were further analyzed for MMM applications. We finally note that computational screening studies aim to identify the "possible top materials" to guide the experimental works, and structural stability of MOFs can only be guaranteed by the experiments. Even if a MOF is experimentally reported to be stable in the absence of the solvent and computationally identified as the top promising material for a target gas separation application, it may decompose under practical applications of membranes such as exposure to air and/or impurities in the gas mixtures.

Results so far demonstrated that MOF membranes offer high H_2 permeabilities, but they have limited H_2/N_2 selectivities compared to the polymeric membranes. Motivated from this, we focused on an alternative usage of MOFs in membrane-based H_2/N_2 separation and examined the effect of using MOFs as fillers in polymers to make MMMs. MMMs merge the benefits of polymers, low cost and proven polymer membrane technology, with those of MOFs, high gas permeabilities.[67−69] Fabrication of MOF-based polymer membranes can readily be envisioned with minor adaptation of the existing commercial technology used for polymeric membranes. Experimental H_2/N_2 separation performance data of six different polymeric membranes that are close to the upper bound were collected from the literature and given in Table S2. These data were then used together with the gas permeability data of the top 13 MOFs obtained from molecular simulations, which were performed at the same conditions with the experimental gas permeance measurements of polymeric membranes.

Figure 7 represents H_2 permeability and H_2/N_2 selectivity of 78 different MOF/polymer MMMs composed of 6 polymers and 13 MOFs and the separation performance data of polymer membranes. H_2 permeabilities of all MOF/polymer MMMs were higher than the corresponding polymeric membranes. The MMMs composed of the polymers having the highest H_2/N_2 selectivities (PBOI-2-Cu^+, 1,1−6FDA-DIA, and NTDA-BAPHFDS(H)) did not show any further improvement in their H_2/N_2 selectivities upon the incorporation of MOF fillers. When MOFs were used as filler in polymers PBOI-2-Cu^+, 1,1−6FDA-DIA, and NTDA-BAPHFDS(H), their H_2

DOI: 10.1021/acssuschemeng.9b01020
ACS Sustainable Chem. Eng. 2019, 7, 9525−9536

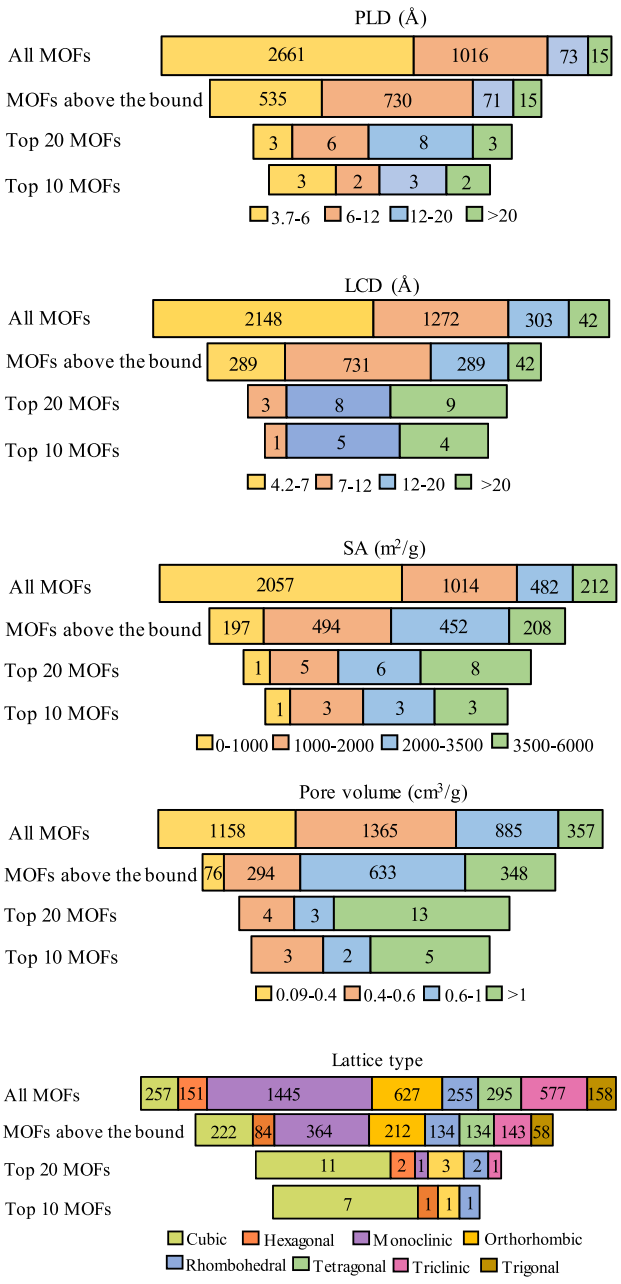


Figure 6. Effects of structural properties, PLD, LCD, SA, pore volume, and lattice type, on the separation performances of the MOF membranes. The numbers represent the number of MOFs categorized in each color-coded box.

permeabilities were significantly increased from 3.7, 31.4, and 52 Barrer to 6.5, 55.2, and 91.4 Barrer, respectively, regardless of the MOF type. Therefore, permeability and selectivity of these MMMs were shown by using a single symbol in Figure 7. Addition of MOF fillers into these polymers leads to MMMs that exceed the Robeson's upper bound. On the other hand, MMMs composed of the other polymers, PIM-1, PIM-7, and PTMSP, showed a variety of permeabilities and selectivities based on the identity of MOF filler. Specifically, H_2 permeabilities of PIM-7, PIM-1, and PTMSP increased from 8.6×10^2, 1.3×10^3, and 2.3×10^4 Barrer to 1.5×10^3, 2.3×10^3, and 4×10^4 Barrer, respectively, with the incorporation of MOF having the highest H_2 permeability (FOTNIN).

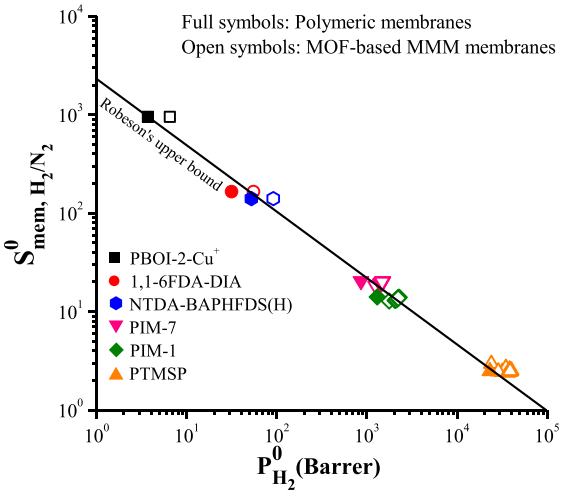


Figure 7. Predicted separation performances of 78 MOF-based MMMs (open symbols) composed of 13 MOFs and 6 polymers. Experimental data for polymeric membranes is shown with full symbols. A single data point was used to represent MMMs composed of PBOI-2-Cu^+, 1,1−6FDA-DIA, and NTDA-BAPHFDS(H) polymers because very similar H_2 permeabilities and H_2/N_2 selectivities were calculated regardless of the identity of the MOF.

Selectivity of these three polymers slightly decreased from 20.5 to 18.4, 14.1 to 12.8, and 2.48 to 2.38 with the addition of MOFs into PIM-7, PIM-1, and PTMSP, respectively. For PTMSP, addition of MOFs, XANLIJ, RUBDUP, XANLEF, PUGPEO, and GUPCUQ01 slightly improved H_2/N_2 selectivity of pure polymer membrane from 2.48 to 2.50, 2.53, 2.57, 2.68, and 2.94, respectively, in addition to the enhancement in H_2 permeability of PTMSP from 2.3×10^4 to 3.9×10^4, 3.9×10^4, 3.8×10^4, 3.5×10^4, and 2.4×10^4 Barrer, respectively. Overall, these calculations showed that incorporating MOFs into polymers almost doubles H_2 permeabilities, and some MOFs even provide slight enhancements in H_2/N_2 selectivities of polymers.

Finally, we discuss the assumptions related with our computational screening work to accurately assess membrane performances of MOFs in practical applications. (i) We used a generic force field, UFF,[37] and an approximate charge assignment method in molecular simulations of MOFs to enable the high-throughput computational screening because development of MOF-specific force fields derived from quantum chemistry calculations is computationally expensive when large numbers of MOFs are considered. The good agreement between experimentally measured and simulated gas permeance results shown in Figure 1 validated the applicability of UFF and the charge assignment method in predicting gas permeances of MOF membranes. We note that force field parameters used in molecular simulations are assumed to be equal to a mean value and subject to uncertainty as discussed in the literature.[70] (ii) We carried out molecular simulations for rigid MOFs, similar to the other high-throughput MOF screening studies in the literature.[22,23,26,27] Our group[31] recently showed that flexibility of structures affects the performance of MOF membranes with pore sizes close to the kinetic diameter of gas molecules. In this work, MOF membranes having pore sizes larger than the kinetic diameter of both gas molecules were considered; therefore, flexibility is expected to have a negligible influence on the predicted separation performances. (iii) We initially performed

DOI: 10.1021/acssuschemeng.9b01020
ACS Sustainable Chem. Eng. 2019, 7, 9525−9536

all molecular simulations of MOFs at infinite dilution for the computational efficiency of our screening process and defined the top MOF candidates based on their performances computed at infinite dilution. However, membranes do not work at infinite dilution and, in fact, pressure is one of the main variables of the membrane-based gas process to optimize the selectivity. Molecular simulations were performed at practical membrane operating conditions, 1 bar and 298 K, considering binary mixtures only for the top MOF candidates. Results given in Figure 4 showed that performing molecular simulations initially at infinite dilution can be an efficient screening approach for identifying the most selective membranes for separation of binary mixtures. (iv) Our molecular simulations do not give insights about the membranes' stability under real operating conditions. MOFs may lose their integrities in the presence of humidity or impurity gases; structural stabilities of MOF membranes can only be guaranteed by further experimental studies. (v) Finally, theoretical calculations assumed a good adhesion between the polymer and MOF phases where several challenges in fabrication of MMMs such as interface void formation, particle sedimentation, and pore blockage were neglected. Computational screening studies help to narrow the candidate materials from thousands to tens, and the issues we discussed above are more likely to be handled by extensive experimental studies on MOF/polymer MMMs.

CONCLUSION

In this study, we investigated performances of MOF membranes for separation of H_2/N_2 mixture. To estimate the separation capabilities of a large number of MOFs in a time efficient manner, we simulated adsorption and diffusion of single-component H_2 and N_2 in 3765 MOFs at infinite dilution and calculated H_2 and N_2 permeabilities as well as H_2/N_2 selectivities of all MOF membranes. A large number of MOF membranes was found to exceed the Robeson's upper bound, offering a good combination of high permeability and moderate selectivity. Considering high H_2 permeabilities of MOFs, we focused on their membrane selectivities to identify the most promising membrane candidates. The top 20 MOFs were identified which have H_2 permeabilities of 3.4×10^4 to 1.7×10^6 Barrer and H_2/N_2 selectivities of 3−7. We then performed GCMC and MD simulations of the top 20 MOFs by considering binary (H_2/N_2) and quaternary ($H_2/N_2/CO_2/CO$) mixtures. Membrane performances calculated at infinite dilution, binary and quaternary mixture conditions were compared. Results showed that molecular simulations performed at infinite dilution generally overestimate H_2/N_2 selectivities and H_2 permeabilities of MOF membranes whereas underestimated their N_2 permeabilities. On the other hand, results of binary mixture simulations were generally in a good agreement with the predicted separation performance of the top 20 membranes under quaternary mixture conditions. Structure−performance relation analysis showed that MOFs having cubic lattice, pore sizes >12 Å, SA >3500 m^2/g, and pore volume >1 cm^3/g showed better performance for H_2/N_2 separation. Finally, we predicted H_2 permeabilities and H_2/N_2 selectivities of MOF/polymer MMMs that are composed of polymers close to the upper bound and MOF fillers. Results showed that incorporation of MOFs into polymers approximately doubles H_2 permeabilities of polymeric membranes and carries them above the upper bound, indicating that MOF/polymer MMMs can advance the current H_2/N_2 separation technologies.

ASSOCIATED CONTENT

Supporting Information

The Supporting Information is available free of charge on the ACS Publications website at DOI: 10.1021/acssuschemeng.9b01020.

Potential parameters of H_2, N_2, CO_2, and CO; experimental gas permeability and selectivity data of polymeric membranes; details of gas permeance measurements of MOF membranes; calculated structural properties of the top 20 MOFs; comments about the structures of the top 20 MOFs; comparison of the membrane-based separation performance of the CSD-deposited and edited MOF structures (PDF)

AUTHOR INFORMATION

Corresponding Author

*E-mail: skeskin@ku.edu.tr; Phone: +90 (212) 338-1362.

ORCID

Seda Keskin: 0000-0001-5968-0336

Notes

The authors declare no competing financial interest.

ACKNOWLEDGMENTS

S.K. acknowledges ERC-2017-Starting Grant. This research received funding from the European Research Council (ERC) under the European Union's Horizon 2020 research and innovation programme (ERC-2017-Starting Grant, Grant 756489-COSMOS).

REFERENCES

(1) Veziroğlu, T. N.; Sahin, S. 21st Century's energy: Hydrogen energy system. *Energy Convers. Manage.* **2008**, *49* (7), 1820−1831.

(2) David, O. C.; Gorri, D.; Nijmeijer, K.; Ortiz, I.; Urtiaga, A. Hydrogen separation from multicomponent gas mixtures containing CO, N_2 and CO_2 using Matrimid® asymmetric hollow fiber membranes. *J. Membr. Sci.* **2012**, *419−420*, 49−56.

(3) Robeson, L. M. The upper bound revisited. *J. Membr. Sci.* **2008**, *320* (1−2), 390−400.

(4) Arratibel, P. A.; Pacheco, T. D.; Van Sint, A. M.; Gallucci, F. Recent advances in Pd-based membranes for membrane reactors. *Molecules* **2017**, *22* (1), 51.

(5) Kang, Z.; Fan, L.; Sun, D. Recent advances and challenges of metal-organic framework membranes for gas separation. *J. Mater. Chem. A* **2017**, *5* (21), 10073−10091.

(6) Adatoz, E.; Avci, A. K.; Keskin, S. Opportunities and challenges of MOF-based membranes in gas separations. *Sep. Purif. Technol.* **2015**, *152*, 207−237.

(7) Lee, D.-J.; Li, Q.; Kim, H.; Lee, K. Preparation of Ni-MOF-74 membrane for CO_2 separation by layer-by-layer seeding technique. *Microporous Mesoporous Mater.* **2012**, *163*, 169−177.

(8) Kang, Z.; Xue, M.; Fan, L.; Huang, L.; Guo, L.; Wei, G.; Chen, B.; Qiu, S. Highly selective sieving of small gas molecules by using an ultra-microporous metal-organic framework membrane. *Energy Environ. Sci.* **2014**, *7* (12), 4053−4060.

(9) Mao, Y.; Shi, L.; Huang, H.; Cao, W.; Li, J.; Sun, L.; Jin, X.; Peng, X. Room temperature synthesis of free-standing HKUST-1 membranes from copper hydroxide nanostrands for gas separation. *Chem. Commun.* **2013**, *49* (50), 5666−5668.

(10) Guo, H.; Zhu, G.; Hewitt, I. J.; Qiu, S. Twin Copper Source" growth of metal-organic framework membrane: $Cu_3(BTC)_2$ with high

permeability and selectivity for recycling H_2. *J. Am. Chem. Soc.* **2009**, *131* (5), 1646−1647.
(11) Nan, J.; Dong, X.; Wang, W.; Jin, W.; Xu, N. Step-by-step seeding procedure for preparing HKUST-1 membrane on porous α-alumina support. *Langmuir* **2011**, *27* (8), 4309−4312.
(12) Ben, T.; Lu, C.; Pei, C.; Xu, S.; Qiu, S. Polymer-supported and free-standing metal-organic framework membrane. *Chem. - Eur. J.* **2012**, *18* (33), 10250−10253.
(13) Stock, N.; Biswas, S. Synthesis of metal-organic frameworks (MOFs): Routes to various MOF topologies, morphologies, and composites. *Chem. Rev.* **2012**, *112* (2), 933−969.
(14) Liu, Y.; Wang, N.; Diestel, L.; Steinbach, F.; Caro, J. MOF membrane synthesis in the confined space of a vertically aligned LDH network. *Chem. Commun.* **2014**, *50* (32), 4225−4227.
(15) Bux, H.; Liang, F.; Li, Y.; Cravillon, J.; Wiebcke, M.; Caro, J. Zeolitic imidazolate framework membrane with molecular sieving properties by microwave-assisted solvothermal synthesis. *J. Am. Chem. Soc.* **2009**, *131* (44), 16000−16001.
(16) Shah, M. N.; Gonzalez, M. A.; McCarthy, M. C.; Jeong, H.-K. An unconventional rapid synthesis of high performance metal-organic framework membranes. *Langmuir* **2013**, *29* (25), 7896−7902.
(17) McCarthy, M. C.; Varela-Guerrero, V.; Barnett, G. V.; Jeong, H.-K. Synthesis of zeolitic imidazolate framework films and membranes with controlled microstructures. *Langmuir* **2010**, *26* (18), 14636−14641.
(18) Huang, A.; Bux, H.; Steinbach, F.; Caro, J. Molecular-sieve membrane with hydrogen permselectivity: ZIF-22 in LTA topology prepared with 3-aminopropyltriethoxysilane as covalent linker. *Angew. Chem., Int. Ed.* **2010**, *49* (29), 4958−4961.
(19) Dong, X.; Huang, K.; Liu, S.; Ren, R.; Jin, W.; Lin, Y. Synthesis of zeolitic imidazolate framework-78 molecular-sieve membrane: Defect formation and elimination. *J. Mater. Chem.* **2012**, *22* (36), 19222−19227.
(20) Huang, A.; Dou, W.; Caro, J. Steam-stable zeolitic imidazolate framework ZIF-90 membrane with hydrogen selectivity through covalent functionalization. *J. Am. Chem. Soc.* **2010**, *132* (44), 15562−15564.
(21) Huang, A.; Caro, J. Covalent post-functionalization of zeolitic imidazolate framework ZIF-90 membrane for enhanced hydrogen selectivity. *Angew. Chem., Int. Ed.* **2011**, *50* (21), 4979−4982.
(22) Li, S.; Chung, Y. G.; Snurr, R. Q. High-throughput screening of metal-organic frameworks for CO_2 capture in the presence of water. *Langmuir* **2016**, *32* (40), 10368−10376.
(23) Qiao, Z.; Zhang, K.; Jiang, J. In silico screening of 4764 computation-ready, experimental metal-organic frameworks for CO_2 separation. *J. Mater. Chem. A* **2016**, *4* (6), 2105−2114.
(24) Altintas, C.; Avci, G.; Daglar, H.; Nemati Vesali Azar, A.; Velioglu, S.; Erucar, I.; Keskin, S. Database for CO_2 separation performances of MOFs based on computational materials screening. *ACS Appl. Mater. Interfaces* **2018**, *10* (20), 17257−17268.
(25) Watanabe, T.; Sholl, D. S. Accelerating applications of metal-organic frameworks for gas adsorption and separation by computational screening of materials. *Langmuir* **2012**, *28* (40), 14114−14128.
(26) Qiao, Z.; Peng, C.; Zhou, J.; Jiang, J. High-throughput computational screening of 137953 metal-organic frameworks for membrane separation of a $CO_2/N_2/CH_4$ mixture. *J. Mater. Chem. A* **2016**, *4* (41), 15904−15912.
(27) Qiao, Z.; Xu, Q.; Jiang, J. High-throughput computational screening of metal-organic framework membranes for upgrading of natural gas. *J. Membr. Sci.* **2018**, *551*, 47−54.
(28) Budhathoki, S.; Ajayi, O.; Steckel, J. A.; Wilmer, C. E. High-throughput computational prediction of the cost of carbon capture using mixed matrix membranes. *Energy Environ. Sci.* **2019**, *12*, 1255.
(29) Altintas, C.; Avci, G.; Daglar, H.; Gulcay, E.; Erucar, I.; Keskin, S. Computer simulations of 4240 MOF membranes for H_2/CH_4 separations: Insights into structure−performance relations. *J. Mater. Chem. A* **2018**, *6* (14), 5836−5847.
(30) Kadioglu, O.; Keskin, S. Efficient separation of helium from methane using MOF membranes. *Sep. Purif. Technol.* **2018**, *191*, 192−199.
(31) Altintas, C.; Keskin, S. Molecular simulations of MOF membranes and performance predictions of MOF/polymer mixed matrix membranes for CO_2/CH_4 separations. *ACS Sustainable Chem. Eng.* **2019**, *7*, 2739−2750.
(32) Avci, G.; Velioglu, S.; Keskin, S. High-throughput screening of MOF adsorbents and membranes for H_2 purification and CO_2 capture. *ACS Appl. Mater. Interfaces* **2018**, *10* (39), 33693−33706.
(33) Daglar, H.; Keskin, S. Computational screening of metal-organic frameworks for membrane-based $CO_2/N_2/H_2O$ separations: Best materials for flue gas separation. *J. Phys. Chem. C* **2018**, *122* (30), 17347−17357.
(34) Moghadam, P. Z.; Li, A.; Wiggin, S. B.; Tao, A.; Maloney, A. G. P.; Wood, P. A.; Ward, S. C.; Fairen-Jimenez, D. Development of a cambridge structural database subset: A collection of metal-organic frameworks for past, present, and future. *Chem. Mater.* **2017**, *29* (7), 2618−2625.
(35) Willems, T. F.; Rycroft, C. H.; Kazi, M.; Meza, J. C.; Haranczyk, M. Algorithms and tools for high-throughput geometry-based analysis of crystalline porous materials. *Microporous Mesoporous Mater.* **2012**, *149* (1), 134−141.
(36) Dubbeldam, D.; Calero, S.; Ellis, D. E.; Snurr, R. Q. RASPA: Molecular simulation software for adsorption and diffusion in flexible nanoporous materials. *Mol. Simul.* **2016**, *42* (2), 81−101.
(37) Rappé, A. K.; Casewit, C. J.; Colwell, K. S.; Goddard, W. A.; Skiff, W. M. UFF, a full periodic table force field for molecular mechanics and molecular dynamics simulations. *J. Am. Chem. Soc.* **1992**, *114* (25), 10024−10035.
(38) Keskin, S.; Liu, J.; Rankin, R. B.; Johnson, J. K.; Sholl, D. S. Progress, opportunities, and challenges for applying atomically detailed modeling to molecular adsorption and transport in metal-organic framework materials. *Ind. Eng. Chem. Res.* **2009**, *48* (5), 2355−2371.
(39) Wilmer, C. E.; Snurr, R. Q. Towards rapid computational screening of metal-organic frameworks for carbon dioxide capture: Calculation of framework charges via charge equilibration. *Chem. Eng. J.* **2011**, *171* (3), 775−781.
(40) Rappe, A. K.; Goddard III, W. A. Charge equilibration for molecular dynamics simulations. *J. Phys. Chem.* **1991**, *95* (8), 3358−3363.
(41) Makrodimitris, K.; Papadopoulos, G. K.; Theodorou, D. N. Prediction of permeation properties of CO_2 and N_2 through silicalite via molecular simulations. *J. Phys. Chem. B* **2001**, *105* (4), 777−788.
(42) Buch, V. Path integral simulations of mixed para-D_2 and ortho-D_2 clusters: The orientational effects. *J. Chem. Phys.* **1994**, *100* (10), 7610−7629.
(43) Altintas, C.; Erucar, I.; Keskin, S. High-throughput computational screening of the metal organic framework database for CH_4/H_2 separations. *ACS Appl. Mater. Interfaces* **2018**, *10* (4), 3668−3679.
(44) Liu, J. C.; Rankin, R. B.; Johnson, J. K. The importance of charge-quadrupole interactions for H_2 adsorption and diffusion in Cu-BTC. *Mol. Simul.* **2009**, *35* (1−2), 60−69.
(45) Fischer, M.; Hoffmann, F.; Fröba, M. Metal-organic frameworks and related materials for hydrogen purification: Interplay of pore size and pore wall polarity. *RSC Adv.* **2012**, *2* (10), 4382−4396.
(46) Gu, C.; Gao, G. H.; Yu, Y. X.; Nitta, T. Simulation for separation of hydrogen and carbon monoxide by adsorption on single-walled carbon nanotubes. *Fluid Phase Equilib.* **2002**, *194−197*, 297−307.
(47) Straub, J. E.; Karplus, M. Molecular dynamics study of the photodissociation of carbon monoxide from myoglobin: Ligand dynamics in the first 10 ps. *Chem. Phys.* **1991**, *158* (2−3), 221−248.
(48) Potoff, J. J.; Siepmann, J. I. Vapor-liquid equilibria of mixtures containing alkanes, carbon dioxide, and nitrogen. *AIChE J.* **2001**, *47* (7), 1676−1682.
(49) Evans, D. J.; Holian, B. L. The Nose-Hoover thermostat. *J. Chem. Phys.* **1985**, *83* (8), 4069−4074.

DOI: 10.1021/acssuschemeng.9b01020
ACS Sustainable Chem. Eng. 2019, 7, 9525−9536

(50) Choi, S. H.; Brunetti, A.; Drioli, E.; Barbieri, G. H_2 separation from H_2/N_2 and H_2/CO mixtures with co-polyimide hollow fiber module. *Sep. Sci. Technol.* **2010**, *46* (1), 1−13.
(51) Polotskaya, G.; Goikhman, M.; Podeshvo, I.; Kudryavtsev, V.; Pientka, Z.; Brozova, L.; Bleha, M. Gas transport properties of polybenzoxazinoneimides and their prepolymers. *Polymer* **2005**, *46* (11), 3730−3736.
(52) Rezac, M. E.; Schöberl, B. Transport and thermal properties of poly(ether imide)/acetylene-terminated monomer blends. *J. Membr. Sci.* **1999**, *156* (2), 211−222.
(53) Tanaka, K.; Islam, M. N.; Kido, M.; Kita, H.; Okamoto, K.-I. Gas permeation and separation properties of sulfonated polyimide membranes. *Polymer* **2006**, *47* (12), 4370−4377.
(54) Budd, P. M.; Msayib, K. J.; Tattershall, C. E.; Ghanem, B. S.; Reynolds, K. J.; McKeown, N. B.; Fritsch, D. Gas separation membranes from polymers of intrinsic microporosity. *J. Membr. Sci.* **2005**, *251* (1−2), 263−269.
(55) Nagai, K.; Higuchi, A.; Nakagawa, T. Gas permeability and stability of poly(1-trimethylsilyl-1-propyne-co-1-phenyl-1-propyne) membranes. *J. Polym. Sci., Part B: Polym. Phys.* **1995**, *33* (2), 289−298.
(56) Maxwell, J. C. *A Treatise on Electricity and Magnetism*; Dover Publications: 1954.
(57) Erucar, I.; Keskin, S. Computational screening of metal organic frameworks for mixed matrix membrane applications. *J. Membr. Sci.* **2012**, *407*, 221−230.
(58) Yilmaz, G.; Keskin, S. Molecular modeling of MOF and ZIF-filled MMMs for CO_2/N_2 separations. *J. Membr. Sci.* **2014**, *454*, 407−417.
(59) Bouma, R.; Checchetti, A.; Chidichimo, G.; Drioli, E. Permeation through a heterogeneous membrane: The effect of the dispersed phase. *J. Membr. Sci.* **1997**, *128* (2), 141−149.
(60) Sumer, Z.; Keskin, S. Adsorption- and membrane-based CH_4/N_2 separation performances of MOFs. *Ind. Eng. Chem. Res.* **2017**, *56* (30), 8713−8722.
(61) Guan, G.; Kusakabe, K.; Morooka, S. Gas permeation properties of ion-exchanged LTA-type zeolite membranes. *Sep. Sci. Technol.* **2001**, *36* (10), 2233−2245.
(62) Masuda, T.; Fukumoto, N.; Kitamura, M.; Mukai, S. R.; Hashimoto, K.; Tanaka, T.; Funabiki, T. Modification of pore size of MFI-type zeolite by catalytic cracking of silane and application to preparation of H_2-separating zeolite membrane. *Microporous Mesoporous Mater.* **2001**, *48* (1−3), 239−245.
(63) Kalipcilar, H.; Bowen, T. C.; Noble, R. D.; Falconer, J. L. Synthesis and separation performance of SSZ-13 zeolite membranes on tubular supports. *Chem. Mater.* **2002**, *14* (8), 3458−3464.
(64) Yoshinari, N.; Kakuya, A.; Lee, R.; Konno, T. Parity-controlled self-assembly of supramolecular helices in a gold (I)-copper (II) coordination system with penicillamine and bis(diphenylphosphino) alkane. *Bull. Chem. Soc. Jpn.* **2015**, *88* (1), 59−68.
(65) Allen, F. H. The cambridge structural database: A quarter of a million crystal structures and rising. *Acta Crystallogr., Sect. B: Struct. Sci.* **2002**, *58* (3), 380−388.
(66) Macrae, C. F.; Edgington, P. R.; McCabe, P.; Pidcock, E.; Shields, G. P.; Taylor, R.; Towler, M.; van de Streek, J. Mercury: Visualization and analysis of crystal structures. *J. Appl. Crystallogr.* **2006**, *39* (3), 453−457.
(67) Erucar, I.; Keskin, S. Computational methods for MOF/polymer membranes. *Chem. Rec.* **2016**, *16* (2), 703−718.
(68) Jeazet, H. B. T.; Staudt, C.; Janiak, C. Metal-organic frameworks in mixed-matrix membranes for gas separation. *Dalton Trans.* **2012**, *41* (46), 14003−14027.
(69) Babu, D. J.; He, G.; Villalobos, L. F.; Agrawal, K. V. Crystal engineering of metal-organic framework thin films for gas separations. *ACS Sustainable Chem. Eng.* **2019**, *7* (1), 49−69.
(70) Ricardez-Sandoval, L. A. Current challenges in the design and control of multiscale systems. *Can. J. Chem. Eng.* **2011**, *89* (6), 1324−1341.
(71) Dong, X.; Huang, K.; Liu, S.; Ren, R.; Jin, W.; Lin, Y. S. Synthesis of zeolitic imidazolate framework-78 molecular-sieve membrane: Defect formation and elimination. *J. Mater. Chem.* **2012**, *22* (36), 19222−19227.
(72) Huang, A.; Chen, Y.; Wang, N.; Hu, Z.; Jiang, J.; Caro, J. A highly permeable and selective zeolitic imidazolate framework ZIF-95 membrane for H_2/CO_2 separation. *Chem. Commun.* **2012**, *48* (89), 10981−10983.
(73) Liu, Y.; Ng, Z.; Khan, E. A.; Jeong, H.-K.; Ching, C.-B.; Lai, Z. Synthesis of continuous MOF-5 membranes on porous α-alumina substrates. *Microporous Mesoporous Mater.* **2009**, *118* (1), 296−301.

DOI: 10.1021/acssuschemeng.9b01020
ACS Sustainable Chem. Eng. 2019, 7, 9525−9536